

this structure, it breaks the O-O bond, leaving one O attached to the rest atom, while the other is inserted into a back bond of one of the two adatoms [the lowest energy position of an O atom bonded to an adatom (10)], leaving the second adatom intact. Thermal decomposition of the DD site also gives the same products.

REFERENCES AND NOTES

1. Ph. Avouris, *J. Phys. Chem.* **94**, 2246 (1990); J. Boland, *Adv. Phys.* **42**, 129 (1993).
2. Ph. Avouris, *Acc. Chem. Res.* **28**, 95 (1995).
3. I.-W. Lyo and Ph. Avouris, *Science* **253**, 173 (1991); A. Kobayashi, F. Grey, E. Snyder, M. Aono, *Phys. Rev. B* **49**, 8067 (1994).
4. R. S. Becker, G. S. Higashi, Y. J. Chabal, A. J. Becker, *Phys. Rev. Lett.* **65**, 1917 (1990); J. Wintterlin and Ph. Avouris, *J. Chem. Phys.* **100**, 687 (1994); T.-C. Shen *et al.*, *Science* **268**, 1590 (1995).
5. T. Engel, *Surf. Sci. Rep.* **18**, 91 (1993).
6. G. Hollinger and F. J. Himpsel, *Phys. Rev. B* **28**, 3651 (1983).
7. H. Ibach, H. D. Bruchmann, H. Wagner, *Appl. Phys. A* **29**, 113 (1982).
8. K. Edamoto, Y. Kubota, H. Kobayashi, M. Onchi, M. Nishijima, *J. Chem. Phys.* **83**, 428 (1985).
9. I. P. Batra, P. S. Bagus, K. Hermann, *Phys. Rev. Lett.* **52**, 384 (1984).
10. X. M. Zheng and P. L. Cao, *Surf. Sci.* **219**, L543 (1989).
11. B. Schubert, Ph. Avouris, R. Hoffmann, *J. Chem. Phys.* **98**, 7606 (1993).
12. A. J. Schell-Sorokin and J. E. Demuth, *Surf. Sci.* **157**, 273 (1985).
13. U. Höfer, P. Morgen, W. Wurth, E. Umbach, *Phys. Rev. B* **40**, 1130 (1989).
14. Ph. Avouris, I.-W. Lyo, F. Bozso, *J. Vac. Sci. Technol. B* **9**, 424 (1991).
15. F. Bozso and Ph. Avouris, *Phys. Rev. B* **44**, 9129 (1991).
16. G. Dujardin *et al.*, *Phys. Rev. Lett.* **73**, 1727 (1994).
17. P. Bratu, K. L. Kompa, U. Höfer, *Phys. Rev. B* **49**, 14070 (1994).
18. G. Comtet *et al.*, *Surf. Sci.* **331-333**, 370 (1994).
19. C. Silvestre and M. Shayegan, *Phys. Rev. B* **37**, 10432 (1988).
20. Ph. Avouris and R. Wolkow, *ibid.* **39**, 5071 (1989).
21. J. Tersoff and D. R. Hamann, *ibid.* **31**, 805 (1994).
22. A. Zangwill, *Physics at Surfaces* (Cambridge Univ. Press, Cambridge, 1988).
23. Y. Ono, M. Tabe, H. Kageshima, *Phys. Rev. B* **48**, 14291 (1993).
24. G. J. Schulz, *Rev. Mod. Phys.* **45**, 423 (1973).
25. L. Sanche, *Phys. Rev. B* **23**, 1597 (1990).
26. H. Kuhlbeck *et al.*, *Chem. Phys. Lett.* **238**, 93 (1995).
27. B. Schubert, Ph. Avouris, R. Hoffmann, *J. Chem. Phys.* **98**, 7593 (1993).
28. J. E. Demuth, D. Schmeisser, Ph. Avouris, *Phys. Rev. Lett.* **47**, 1166 (1981).
29. J. W. Gadzuk, L. J. Richter, S. A. Buntin, D. S. King, R. R. Cavanagh, *Surf. Sci.* **235**, 317 (1990); C. P. Salam, M. Persson, R. E. Palmer, *Phys. Rev. B* **49**, 10655 (1994).
30. Ph. Avouris and I.-W. Lyo, in *Scanning Probe Microscopy*, H. K. Wickramasinghe, Ed. (AIP Conference Proceedings 241, American Institute of Physics, New York, 1992).
31. W. A. Goddard III, A. Redondo, T. C. McGill, *Solid State Commun.* **18**, 981 (1976).
32. J. P. Pelz and R. H. Koch, *J. Vac. Sci. Technol. B* **9**, 775 (1991).
33. Ph. Avouris and D. Cahill, *Ultramicroscopy* **42**, 838 (1992).
34. J. E. Northrup, *Phys. Rev. Lett.* **57**, 154 (1986).
35. R.M. acknowledges the receipt of a Fonds pour la Formation de Chercheurs et l'Aide à la Recherche (FCAR) Québec postdoctoral fellowship.

31 August 1995; accepted 22 February 1996

Spatiotemporal Chaos in Electroconvection

Michael Dennin, Guenter Ahlers,* David S. Cannell

Spatiotemporal chaos (STC) near the onset of electroconvection in a nematic liquid crystal is reported. In samples with conductivities greater than 1×10^{-8} per ohm per meter, STC was found to evolve by means of a supercritical Hopf bifurcation from the uniform conduction state. Because this example of STC resulted from nonlinear interactions between only four modes, it provides a realistic opportunity to understand the observed phenomena in terms of a weakly nonlinear theory in the form of four coupled complex Ginzburg-Landau equations derived from the full equations of motion of the system. For smaller conductivities, the pattern immediately above onset consisted of localized pulses of convection that coexisted with the conduction state. The pulses had a unique width in the direction perpendicular to the director (the axis parallel to the average orientation) and had much larger and varying lengths parallel to the director.

Under nonequilibrium conditions, a spatially extended system often undergoes a transition from a uniform state to a state with spatial variation. We refer to this variation as a pattern. In nature, pattern formation is found in such diverse systems as cloud structures, snowflakes, flames, animal skins, and evolving populations. A fascinating aspect of patterns is that many of them have a universal character; physical, chemical, and biological systems all exhibit patterns that have many features in common. A deeper understanding of these features will help us to prevent undesirable patterns (or promote advantageous ones) in physical processes that affect our environment. From the viewpoint of fundamental science, patterns are of interest because their formation is generally associated with nonlinear effects, which lead to qualitatively new phenomena that do not occur in linear systems. Among the most fascinating of these phenomena is STC (1).

The elucidation of STC has been a main goal in nonlinear science since the mid-1970s, when it was first studied in fluid-mechanical systems (2). Loosely, we use the term STC to describe a deterministic system that has irregular variation and is unpredictable in detail, both in space and in time. Most known examples of STC occur as a result of a transition (or bifurcation) from a base state that already has an intricate but nonchaotic spatial variation. A theoretical analysis of STC is very difficult because it must begin at this already complicated starting point.

Here, we describe experimental observations of STC that (over a certain parameter range) evolves directly from the uniform state as the system is pushed beyond the first bifurcation. The STC consists of a superposition of four modes (see below)

that have spatially and temporally varying amplitudes with a mean square that grows continuously from 0 and whose time average is uniformly extended in space. In this case, it should be possible to elucidate the STC by weakly nonlinear theories that are applicable when amplitudes are small. These theories are well developed in the form of so-called complex Ginzburg-Landau (CGL) equations. Because the STC state evolves continuously from the uniform state, and because it consists of only a small number of modes, the relevant coupled CGL equations should be derivable from the full equations of motion (3) of the system (4). An example of the STC state at one instant of time is given in Fig. 1A.

We studied electroconvection (5) in the nematic liquid crystal (NLC) 4-ethyl-2-fluoro-4'-[2-(trans-4-pentylcyclohexyl)ethyl]-biphenyl (I52). The long, rodlike NLC molecules are orientationally ordered relative to their neighbors, but their centers of mass have no positional order. The axis parallel to the average orientation is called the director \hat{n} . We obtained a sample with uniform planar alignment of \hat{n} (parallel to the surfaces) by confining the NLC between two treated parallel glass plates. We used transparent conducting films on the inner surfaces of the glass plates and applied an ac voltage of amplitude V and frequency f between them. At a critical value V_c , a transition from a spatially uniform quiescent state to convection occurs. The precise value of V_c can be altered by changing f or by changing the electrical conductivity σ ; the conductivity can be changed either by adding small amounts of iodine to the I52 or by changing the temperature. Values of σ in our samples ranged from 0.6×10^{-8} to 1.8×10^{-8} ohm $^{-1}$ m $^{-1}$.

Immediately above V_c and for $\sigma \approx 1 \times 10^{-8}$ ohm $^{-1}$ m $^{-1}$, we found oblique rolls with a wave vector \mathbf{k} at a nonzero angle θ with respect to \hat{n} (6, 7). Because \hat{n} only gives an axis and does not specify a direc-

Department of Physics and Center for Nonlinear Science, University of California, Santa Barbara, CA 93106, USA.

*To whom correspondence should be addressed.

tion along it, the states with angles θ and $\pi - \theta$ have an equal a priori likelihood of occurring. We refer to these states as “zig” and “zag” rolls, respectively. The rolls traveled in the direction of \mathbf{k} or $-\mathbf{k}$, thus providing a time dependence with frequency ω . The right- and left-traveling zig and zag rolls constitute the four modes mentioned above. The parameters V_c , \mathbf{k} , and ω depend only on the linear terms in the equations of motion (3). They have been calculated as a function of σ and f and are in excellent agreement with experiment (6). Interactions between the modes lead to a wealth of nonlinear states as a function of V , σ , and f . We studied patterns in the weakly nonlinear regime where the control parameter $\varepsilon \equiv (V^2 - V_c^2)/V_c^2$ is less than 0.1, and for $f = 25$ Hz.

The apparatus (7) consisted of a computer-controlled shadowgraph imaging system, electronics for applying the ac voltage and measuring the conductivity of the samples, and a sample stage with a temperature range of 30° to 60°C (stability, ± 1 mK). The cell thickness was $d = 28 \pm 2$ μm , uniform to ± 0.5 μm . We varied the conductivity by varying the temperature (6). The sample area was 0.5 cm by 0.5 cm, and a central part of this area was imaged with light polarized parallel to \hat{n} . In the following discussion, the directions parallel and perpendicular to \hat{n} are sometimes referred to as the x and y axes, respectively. The wavelength of the rolls was $\sim 1.5d$ (42 μm), and the frequency of the traveling waves was close to 1 Hz.

A snapshot of the STC state for $\sigma = 1.5 \times 10^{-8}$ $\text{ohm}^{-1} \text{m}^{-1}$ and $\varepsilon = 0.01$ is shown in Fig. 1A. The irregular spatial variation of the roll envelopes is apparent. The spatial power spectrum of Fig. 1A (the square of the modulus of its Fourier transform) is given in Fig. 1B. The four peaks corresponding to the zig and zag modes can clearly be seen. Although it is not evident from the image, the pattern consists of relatively fast traveling waves of convection rolls, and (on a time scale much longer than a traveling-wave period) the envelopes of the rolls fluctuate irregularly in both space and time.

The spatial and temporal average of the mean square amplitude Θ^2 of the deviation of the director from planar alignment is shown in Fig. 2 as a function of ε . Convection causes Θ^2 to increase for $\varepsilon > 0$ (the small nonzero background value for $\varepsilon < 0$ is the result of fluctuations and instrumental effects). The data do not show any hysteresis near $\varepsilon = 0$. They reveal that the convection amplitude grows continuously from its background value as ε is increased. Thus, the pattern for $\varepsilon > 0$ can be studied for arbitrarily small amplitudes. This feature permits a perturbative theoretical approach

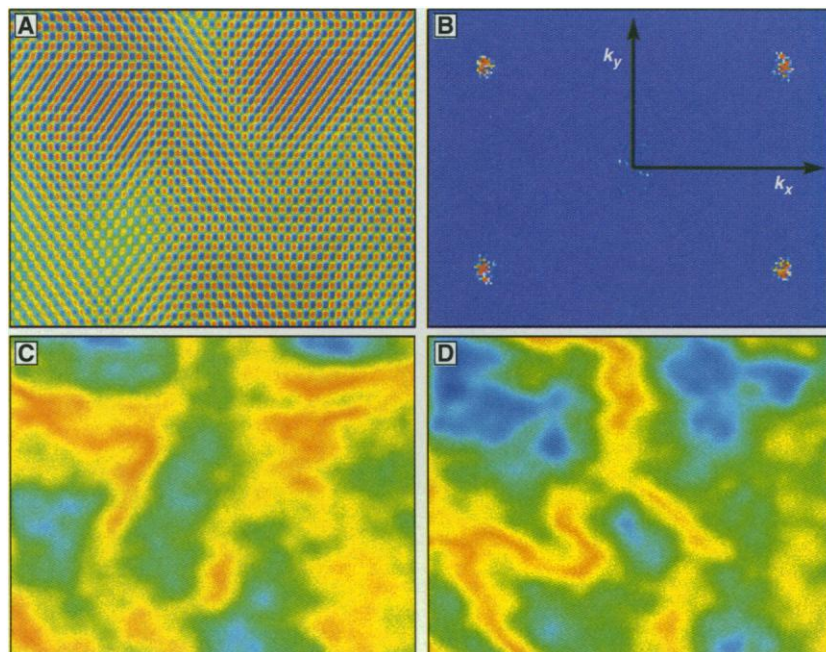


Fig. 1. (A) An example of the spatially extended state of STC for $\sigma = 1.5 \times 10^{-8}$ $\text{ohm}^{-1} \text{m}^{-1}$ and $\varepsilon = 0.01$. The maxima and minima of a shadowgraph signal are mapped to blue and red, respectively. The power spectrum (B), the envelope of the zig rolls (C), and the envelope of the zag rolls (D) are shown for the example in (A). For the power spectrum (B), zero is mapped to blue and the maximum to red. For the envelopes (C and D), the minima are mapped to red and the maxima to blue. The image covers an area of about 0.22 cm by 0.17 cm; \hat{n} is horizontal.

and the derivation of relevant CGL equations from the full equations of motion.

To extract more detail from the experiment, we expressed the right- and left-traveling zig and zag rolls as $A_n(\mathbf{x}, t) \cos(\mathbf{k}_n \mathbf{x} - \omega_n t)$ ($n = 1, 2, 3, 4$), where \mathbf{x} is the horizontal position vector, and $|\mathbf{k}_n| \approx 4.1/d$ and $|\omega_n| \approx 6.3 \text{ s}^{-1}$ for all four modes. If the x axis points to the right and θ is measured from the positive x axis in the counterclockwise direction, then the angle between \mathbf{k}_n and the director is θ for the zig states and $\pi - \theta$ for the zag states. To study a particular $A_n(\mathbf{x}, t)$, we demodulated the images by Fourier-transforming them in space and time, with the transform set to 0 everywhere except for a small region around the

\mathbf{k}_n and ω_n of interest. Taking the inverse transform gives a complex function of space and time; the real part corresponds to $A_n(\mathbf{x}, t) \cos(\mathbf{k}_n \mathbf{x} - \omega_n t)$, and the modulus is the desired amplitude $A_n(\mathbf{x}, t)$. Typical examples of the amplitudes of the zig and zag modes at one moment in time are shown in Fig. 1, C and D.

Various analyses of the mode amplitudes were carried out for $\sigma = 1.5 \times 10^{-8}$ $\text{ohm}^{-1} \text{m}^{-1}$. For $\varepsilon = 0.01$, the spatial correlation length of $A_n(\mathbf{x}, t)$ was found to be $\xi_{\parallel} = 25\lambda$ in the direction of \hat{n} (where $\lambda = 2\pi/|\mathbf{k}|$ is the pattern wavelength) and $\xi_{\perp} = 20\lambda$ perpendicular to \hat{n} . We also characterized the STC by taking a time series of images with a spatial extent $l \approx 4\lambda$, which is much less than ξ_{\parallel} or ξ_{\perp} . Each image was demod-

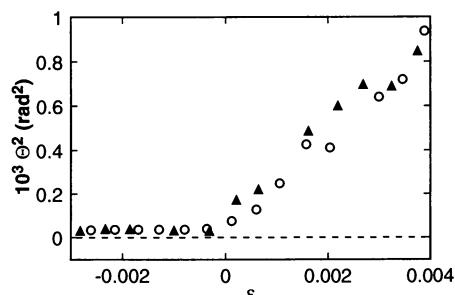


Fig. 2. Mean square amplitude Θ^2 of the deviation of the director from planar alignment as a function of ε ($= 1.5 \times 10^{-8}$ $\text{ohm}^{-1} \text{m}^{-1}$). The symbols \circ and \blacktriangle correspond to data taken with increasing and decreasing ε , respectively.

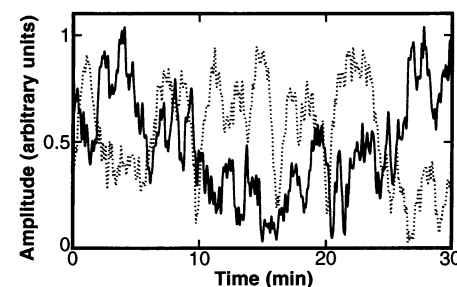


Fig. 3. Temporal variation of the amplitude of the right-traveling zig (solid line) and zag (dashed line) rolls in a small region of the cell. The data are for $\sigma = 1.5 \times 10^{-8}$ $\text{ohm}^{-1} \text{m}^{-1}$ and $\varepsilon = 0.01$.

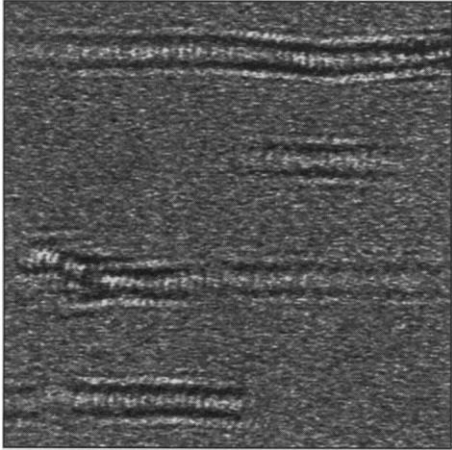


Fig. 4. An example of the localized structures for $\sigma = 0.6 \times 10^{-8} \text{ ohm}^{-1} \text{ m}^{-1}$ and $\varepsilon = 0.05$. The image covers an area of 0.17 cm by 0.17 cm.

ulated, yielding an amplitude that varied only slightly over the image. The spatial average $A_n(t)$ was then studied separately for the four modes. A 30-min segment of $A_n(t)$ for the right-traveling zig and zag rolls for $\varepsilon = 0.01$ is shown in Fig. 3. At times one of the modes dominates, and at other times the modes have approximately equal amplitudes. Computation of the cross-correlation of pairs of the $A_n(t)$ from a 4-hour time series showed that the four modes are anti-correlated with each other. The autocorrelation time of a single $A_n(t)$ was roughly $1000\tau_d$ for all four modes [where $\tau_d = \mathcal{O}(1 \text{ s})$ is the director relaxation time]. This state persisted for the duration of the experiment (>48 hours).

Qualitatively different chaotic phenomena occur in this system when σ is small. For $\sigma = 0.6 \times 10^{-8} \text{ ohm}^{-1} \text{ m}^{-1}$, we observed no evidence of any spatially extended STC. Instead, highly localized elongated convective structures or pulses, consisting of traveling waves under a slowly moving envelope, coexisted with regions of pure conduction up to $\varepsilon \approx 0.1$. Because of their spatial and temporal appearance, we refer to these pulses as “worms.” An example is shown in Fig. 4 for $\varepsilon = 0.05$. In the direction perpendicular to \hat{n} , the worms had a unique width equal to a few times λ . Parallel to \hat{n} , they had a distribution of lengths.

An exciting prospect for the future is to compare quantitative, experimentally determined statistical measures of these states with calculations based on the equations of motion of this system. Calculations based on weakly nonlinear theory should be possible because the experiment (see Fig. 2) indicates that the mean-square amplitudes of the chaotic states grow continuously from 0 as the system is driven further from equilibrium and because only a small number of modes is involved in the spatiotemporal complexity. Such a comparison may

yield useful insights into the nature of STC. It remains to be seen to what extent the lessons learned from this specific system can be applied to STC in general.

REFERENCES AND NOTES

1. M. C. Cross and P. C. Hohenberg, *Rev. Mod. Phys.* **65**, 851 (1993); *Science* **263**, 1569 (1994).
2. G. Ahlers, *Phys. Rev. Lett.* **33**, 1185 (1974); J. P. Gollub and H. L. Swinney, *ibid.* **35**, 927 (1975).
3. M. Treiber and L. Kramer, *Mol. Cryst. Liq. Cryst.* **261**, 311 (1995).
4. Another system in which STC evolves from the uniform state by means of a supercritical bifurcation is convection in an isotropic fluid with rotation about a vertical axis [G. Küppers and D. Lortz, *J. Fluid Mech.* **35**, 609 (1969)]. However, in this case it is not clear that the system can be described by a small number of modes and the corresponding coupled Ginzburg-Landau equations. Attempts to do so have led to disagreement with experimental results [Y. Hu, R. E. Ecke, G. Ahlers, *Phys. Rev. Lett.* **74**, 5040 (1995) and references therein].
5. For a recent review of pattern formation in liquid crystals, see L. Kramer and W. Pesch, *Annu. Rev. Fluid Mech.* **27**, 515 (1995).
6. M. Dennin, M. Treiber, L. Kramer, G. Ahlers, D. S. Cannell, *Phys. Rev. Lett.* **76**, 319 (1996).
7. M. Dennin, G. Ahlers, D. S. Cannell, in *Spatio-Temporal Patterns*, P. E. Cladis and P. Muhoray, Eds. (Addison-Wesley, Reading, MA, 1994), pp. 353–365.
8. Supported by NSF grant DMR94-19168.

23 October 1995; accepted 16 February 1996

Continental Crust, Crustal Underplating, and Low-Q Upper Mantle Beneath an Oceanic Island Arc

Kiyoshi Suyehiro,* Narumi Takahashi, Yoshiro Ariie, Yasutaka Yokoi, Ryota Hino, Masanao Shinohara, Toshihiko Kanazawa, Naoshi Hirata, Hidekazu Tokuyama, Asahiko Taira

A detailed structural model of the crust, subducting slab, and underlying upper mantle across the northern Izu-Ogasawara (Bonin) island arc system is derived from a marine seismic reflection and ocean bottom seismographic refraction survey and subsequent forward modeling combined with tomographic inversion. The model indicates that the crust is thickest beneath the presently active rift zone and a granitic crust may have formed in the mid-crust. A highly attenuative mantle (that is, one with low quality Q) seems to be confined mainly beneath the presently active rift zone. In contrast, high P -wave velocity persists in the lower crust between the forearc and eastern margin of the back arc basin, suggesting a large-scale magma input responsible for the arc formation.

Oceanic island arcs (OIAs) develop at oceanic plate boundaries, where one plate is subducted below the other. The subduction produces intense igneous activity below the overriding plate, leading to the formation of a volcanic arc. Eventually, the volcanic arc may accrete to a continent and become a component of the continental crust. This connection to the continental crust has led some workers to suggest that continental crust formation began at OIAs in the early history of the Earth (1). In addition, the mechanisms of subduction, melt initiation, slab dehydration, and arc volcanism at OIAs are poorly understood. Modeling the seismic structure of the OIA crust, in order

to constrain the volume and type of crustal accretion and its composition, particularly in the deeper crust, of which very little is known, is essential to understanding OIA evolution and its role in the growth of continental crust.

The Izu-Ogasawara arc system located off the southern coast of Japan, extending more than 1000 km from north to south, is a site of active rifting and subduction (Fig. 1) (2, 3). The arc formation was probably initiated at an intraoceanic transform fracture zone boundary about 48 million years ago (Ma) (4). The initial arc volcanism, characterized by tholeiite and boninite lavas, created an arc 300 to 450 km wide. Rifting during the Oligocene formed the forearc and back arc basins, which resulted in the spreading of the Shikoku Basin (until 15 Ma) and the separation of Kyushu-Palau Ridge. The arc volcanism revived about 17 Ma and intensified about 2 Ma, creating the present-day volcanic front (VF), including occasional forearc volcanic intrusions and chains of volcanoes that obliquely cross the

K. Suyehiro, N. Takahashi, Y. Ariie, Y. Yokoi, H. Tokuyama, A. Taira, Ocean Research Institute, University of Tokyo, Tokyo 164, Japan.

R. Hino, Faculty of Science, Tohoku University, Sendai 981, Japan.

M. Shinohara, Department of Earth Sciences, Chiba University, Chiba 263, Japan.

T. Kanazawa and N. Hirata, Earthquake Research Institute, University of Tokyo, Tokyo 113, Japan.

*To whom correspondence should be addressed.